Near-barrier fusion and total reaction of a proton-rich projectile: ^{3}He+^{58}Ni

E. F. Aguilera,* E. Martinez-Quiroz, R. Chávez-González, P. Amador-Valenzuela, D. Lizcano, and A. Gómez-Camacho
Departamento de Aceleradores, Instituto Nacional de Investigaciones Nucleares, Apartado Postal 18-1027, Código Postal 11801, México, Distrito Federal, México

J. J. Kolata, L. O. Lamm,† A. Roberts, and T. Spencer
Physics Department, University of Notre Dame, Notre Dame, Indiana 46556-5670, USA

F. D. Becchetti, H. Jiang, and M. Ojaruega
Physics Department, University of Michigan, Ann Arbor, Michigan 48109-1120, USA

P. A. DeYoung
Department of Physics and Engineering, Hope College, Holland, Michigan 49423-9000, USA

G. F. Peaslee
Department of Chemistry, Hope College, Holland, Michigan 49423-9000, USA

J. Brown
Physics Department, Wabash College, P.O. Box 353, Crawfordsville, Indiana 47933, USA
(Received 20 August 2012; revised manuscript received 24 November 2012; published 22 January 2013)

Evaporation protons from the fusion of the ^{3}He+^{58}Ni system were measured at three energies near but above the Coulomb barrier. The respective elastic scattering angular distribution was also determined for one of these energies. The fusion data, after being properly reduced to eliminate size and charge effects, are compared to the recently measured fusion excitation function for the proton-halo system ^{8}B+^{58}Ni. As a reference, fusion data for the ^{16}O+^{58}Ni system are also presented. With respect to this reference, the fusion cross sections for the proton-rich systems show an enhancement likely related to static effects. An excitation function for the respective total-reaction cross section was extracted from the measured elastic data along with additional data from the literature. Surprisingly, this excitation function follows the trend expected for weakly bound systems.

DOI: 10.1103/PhysRevC.87.014613 PACS number(s): 25.55.−e, 25.60.Dz, 25.60.Pj

I. INTRODUCTION

Recent experimental results for the fusion of the exotic proton-halo system ^{8}B+^{58}Ni show a strong enhancement both below and above the Coulomb barrier [1]. This behavior, qualitatively different from the usual sub-barrier enhancement observed for many heavy-ion systems [2–5], has been associated with a possible static effect related to the extended size of the respective proton-halo state [1,6].

However, even though neutron-halo systems do also have extended wave functions, the respective fusion cross sections do not show this kind of enhancement. While fusion tends to saturate the total-reaction cross section at high energies for the above proton-halo system, the corresponding excitation functions, $\sigma_{\rm fus}$(E) and σ_R(E), stay rather parallel to each other in the case of the known data for the neutron-halo projectile ^{6}He [7]. Therefore, in addition to the extended halo size, it is possible that a dynamic effect of Coulomb polarization might also be important in defining the fusion mechanism for halo systems. It has been shown for the case of Coulomb breakup, for instance, that both the halo nature and the Coulomb polarization of the ^{8}B projectile have a strong influence [8].

Under the assumption that the core and halo decouple from each other [9,10], it is reasonable to expect that these Coulomb polarization effects would affect differently the fusion process for the cases of proton- as opossed to neutron-halo projectiles. This would likely explain the mentioned differences in the fusion data. Within this context, the importance (or not) of the true halo character of the ^{8}B projectile can be tested by comparing the fusion cross sections for the proton-halo system to similar data for other proton-rich nuclei.

The ^{3}He nucleus, with a binding energy (5.49 MeV) below the typical value for stable nuclei, is an extreme case of light proton-rich nuclei. It lies on the edge of the proton drip line, at the light-mass end. The present work reports on some fusion measurements for the ^{3}He+^{58}Ni system, performed at three energies near the Coulomb barrier. An elastic scattering angular distribution for the highest energy was also obtained.

Section II reports the experimental procedure, while in Sec. III the results for the evaporation protons are described and the fusion cross sections are deduced; a comparison is also made with fusion data for projectiles of ^{8}B and ^{16}O. The results for the elastic scattering angular distribution are described in Sec. IV along with an optical model analysis including data reported in other work. An excitation function is obtained for

*eli.aguilera@inin.gob.mx
†Deceased.

the total-reaction cross section and a discussion is made of the respective behavior. Finally, a summary and the conclusions of this work are presented in Sec. V.

II. EXPERIMENTAL PROCEDURE

In Ref. [1], the fusion excitation function for the ^{8}B+^{58}Ni system was obtained by detecting the evaporation protons and using the proton multiplicity calculated with the code PACE [11] to deduce the fusion events. The beam was contaminated with ^{3}He and ^{7}Li, which could not be separated from ^{8}B by time of flight. The present experiment, using the same technique to get the respective fusion cross sections for the ^{3}He+^{58}Ni system, served the additional purpose of determining the contribution of the ^{3}He contaminant beam to the proton yield in the above measurements (see Ref. [1]). It was for this purpose that the ^{3}He beam was generated as a secondary beam at the *TwinSol* facility [12] at the University of Notre Dame (UND). ^{3}He primary beams of 16.5, 15.2, and 13.9 MeV, provided by the FN Tandem accelerator at UND, were elastically scattered from a Be foil. This produced secondary beams with laboratory energies at the center of the target of 12.7, 11.5, and 10.2 MeV, respectively. The energy resolution was 890 keV (FWHM). Primary beam currents of ∼20 particle-nA were typically used, yielding secondary beam rates of $\sim 1.0 \times 10^{7}$ s^{-1}.

The targets consisted of foils of enriched ^{58}Ni, with thicknesses of 426 (924) μg/cm^2, used for the measurements at 12.7 and 11.5 MeV (10.2 MeV), respectively. Monitor $\Delta E/E$ telescopes to detect the elastic particles were placed at $+41^\circ$ and -47°, while four detector telescopes, placed at 117°, 132°, 147°, and 162°, were used to detect the evaporation protons. No protons coming from direct reactions are expected at these backward angles. This is consistent with the observed proton spectra, as shown later.

After the first measurements, at 12.7 MeV, data were taken with an empty Al frame identical to the one holding the target. As a result, it became clear that a substantial number of the protons reaching the backward telescopes were being produced by interactions of the beam with the Al frame. The effective beam spot size on the target is actually much smaller (∼2 mm) than the target itself (∼25 mm), but even a faint beam halo hitting the frame can produce many protons. Shielding the target frame with a Ta plate considerably improved the situation. The three energies were then measured using this Ta shield in front of the target, and blank target bombardments were done (keeping the shield) immediately after each of these runs, to determine the contribution of the respective background protons. Care was taken not to modify either the setup or the beam conditions between the measurements with and those without target. Corrections for these background protons were then applied.

The beam particles hitting the Ta shield also produced a thick target backscattering spectrum in the backward telescopes, which fairly masked the elastic peak corresponding to scattering on ^{58}Ni. However, for the run with no Ta shield at 12.7 MeV, kinematics should allow one to separate the elastic peak from the thick target spectrum produced, in this case, by the Al frame. An elastic scattering angular distribution was thus determined at 12.7 MeV.

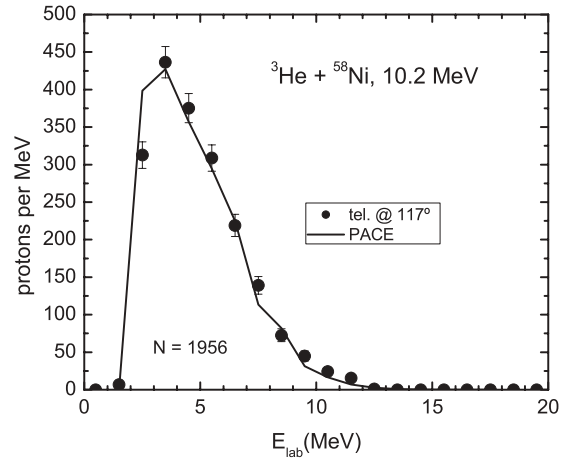

FIG. 1. Typical proton spectrum ($E_{lab} = 10.2$ MeV, $\theta_{lab} = 117^\circ$) compared with a PACE calculation. The latter was normalized to the total number of protons measured, $N = 1956$.

III. PROTON AND FUSION CROSS SECTIONS

A typical proton spectrum is displayed in Fig. 1. It can be seen that the experimental points closely follow the predictions of the evaporation model, computed with the code PACE [11]. This supports the assumption that there is not any important contribution from direct reactions to these spectra.

α particles with $E_\alpha \lesssim 7.5$ MeV will not go through the ΔE detectors of the backward telescopes, whose thicknesses were optimized to resolve protons. So, the respective spectra actually are truncated below this energy. It was checked, however, that the measured portion of the α-particle spectra is consistent with the results of the PACE calculations, as illustrated in Fig. 2. As for neutron emission from the compound nucleus, only the ^{60}Zn(n) and ^{59}Cu(pn) channels may be relevant for the energy region of interest. The first of these gives negligible yields (less than 2% of σ_{fus}) and the latter is already accounted for in the measured proton yield.

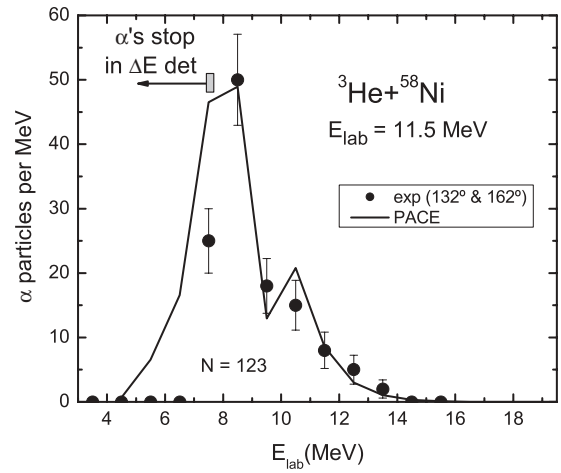

FIG. 2. Typical α spectrum ($E_{lab} = 11.5$ MeV) compared with a PACE calculation. The ΔE detectors, optimized to resolve protons, stopped the lower energy α particles.

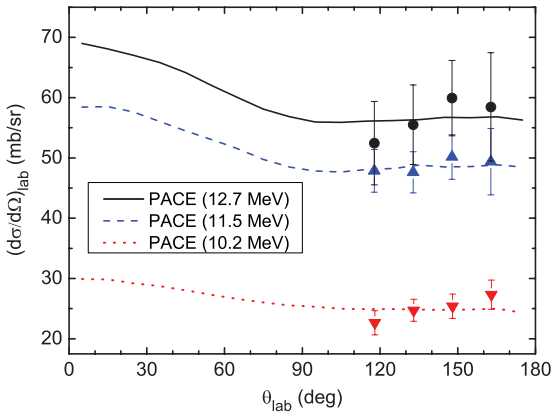

FIG. 3. (Color online) Differential proton cross sections measured (symbols) and corresponding PACE calculations (lines).

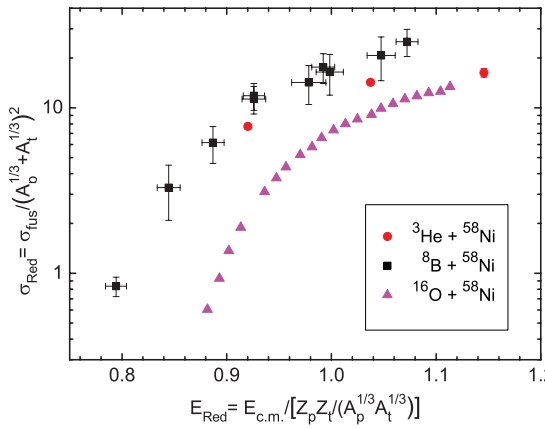

FIG. 4. (Color online) Reduced fusion cross sections from the present work compared with data for other systems.

The proton data in the backward telescopes were normalized to the elastic scattering cross sections measured at the monitors. This is usually assumed to be given by Rutherford's formula, but the energies in the present experiment are actually above the corresponding Coulomb barrier, and the angles of the monitors are not small enough to guarantee pure Coulomb scattering. Although the respective deviations from Rutherford are small, it was checked that all normalizations in the present work were consistent with the elastic scattering analysis presented in Sec. IV. Figure 3 shows the results for the differential proton cross sections, determined for each detector angle at the three energies of the experiment. These results were then extrapolated to lower angles through respective PACE calculations, as displayed by the curves in the figure. Integration of these curves over the whole solid angle gives the total cross sections for evaporation protons, with the results reported in Table I. This table also presents the respective multiplicities, calculated with PACE, which were used to deduce the corresponding fusion cross sections, $\sigma_{\rm fus}$.

In the present work, default values were used for most input parameters in PACE. More specifically, the Yrast line was always determined by the liquid drop rotational energy, the A. J. Sierk fission barrier was assumed throughout the calculations, the level density parameter was $a = A/7.5$ (but the effect of variations in a was investigated, see below), and the regular Wapstra mass table supplied with the code was used for all involved nuclei. In addition, the experimental fusion cross sections were used as an input (in an iterative way), which means that the code internally shifts the respective optical model transmission coefficients to reproduce these values.

Model dependency was tested by varying the level density parameter a within extreme values $(A/10 \leqslant a \leqslant A/7)$ [13]

TABLE I. Integrated cross sections for evaporated protons (σ_p), proton multiplicities (M_p), and deduced fusion cross sections ($\sigma_{\rm fus}$).

$E_{\rm lab}$ (MeV)	$E_{\rm c.m.}$ (MeV)	σ_p (mb)	M_p	$\sigma_{\rm fus}$ (mb)
10.2	9.7	329 ± 13	1.51	218 ± 9
11.5	10.9	636 ± 24	1.58	403 ± 15
12.7	12.1	741 ± 43	1.61	460 ± 27

and by using the alternate parametrization of Gilbert and Cameron [14]. A maximum variation of about ±6% was obtained in the multiplicities. In addition, multiplicity calculations with the code LILITA [15,16] also were performed, yielding a maximum difference of 8% with respect to the results from PACE. The input parameters for LILITA were chosen as to have a meaningful comparison with the PACE calculations. An important difference in these two Monte Carlo codes resides in the way the transmission coefficients T_l are obtained. In PACE T_l's are calculated for the compound-nucleus values of A and Z and an extrapolation is made for subsequent decays by assuming that the respective T_l values are shifted in their kinetic energy dependence [17]. In the version of LILITA used here, explicit calculation of all necessary transmission coefficients is made [16]. Based on the above results, an estimated systematic uncertainty of 8% is assigned to the reported fusion cross sections.

Figure 4 presents a comparison of our results with the fusion excitation functions for two other systems with the same target, where the projectile was either the proton-halo isotope ^{8}B [1] or the tightly bound nucleus ^{16}O [18]. For the purpose of comparing data for different systems, several scaling procedures have been used in the literature, as discussed, for instance, in Refs. [19–21]. Here we chose the prescription recommended in [19], where the cross sections are divided by the quantity r_{pt}^2, with $r_{pt} = A_p^{1/3} + A_t^{1/3}$, while the energies are scaled by the factor Z_pZ_t/r_{pt}. This energy scaling allows one to compare the behavior with respect to a smooth trend of the respective Coulomb barriers, but will not wash out possible structure effects on the barrier (see discussion below for the ^{16}O case). The cross-section reduction eliminates size effects related to a normal $A^{1/3}$ dependence, whithout washing out the effects of possible deviations from this rule, such as may be expected for halo, weakly bound, or very light nuclei. Even though any scaling procedure has associated uncertainties, recently this very simple prescription has proved to be most useful in the comparison of reaction data for a large variety of systems, including data for ^{8}B and ^{16}O [22] or projectiles as light as ^{4}He [10]. A complete survey of these comparisons can be found in Ref. [7] and a brief discussion of the underlying physics is given in Sec. IV.

The fusion cross sections for ^{3}He+^{58}Ni in Fig. 4 are between the other two excitation functions, with the low-energy point approaching the data for the proton-halo system, while the high-energy point approaches the points corresponding to the tightly bound system. With respect to the latter, both proton-rich systems show a fusion enhancement, but with different behavior. A structure effect should be present in the energy scale of Fig. 4 for the ^{16}O+^{58}Ni system. The ^{16}O nucleus has a strong octupole state which produces an appreciable downward shift in the corresponding Coulomb barrier. As discussed in Ref. [18], the overall barrier shift produced in this system by all inelastic and transfer couplings is estimated to be 0.75 MeV, which is only about 2% of the barrier height (31.3 MeV). So, notwithstanding this structure effect, one can say that the ^{16}O+^{58}Ni system is still a good reference for our comparison. There is no way that the qualitatively different energy behavior observed for the ^{3}He projetile or the strong enhancement associated with ^{8}B could be masked by such a 2% effect in the reduced energy scale.

The respective behavior for the ^{8}B+^{58}Ni system possibly results from a static effect owing to the extended size of the proton halo [1]. This would enhance the total-reaction probability throughout the entire energy region, which in turn could favor fusion. Below the barrier, dynamic effects could also contribute to the enhancement [10,23]. For reference, the fusion barrier positions in Fig. 4 correspond to $E_{\rm Red}$ values of 0.84, 0.89, and 0.83 for ^{8}B [1], ^{16}O [18], and ^{3}He, respectively. The latter value was estimated from systematics [2,24,25].

There is evidence that the proton-rich isotope ^{3}He also does show an atypically large interaction radius [26], so the respective σ_R should also be enhanced (evidence is presented in Sec. IV). The behavior observed in Fig. 4 suggests that in this case fusion starts to become favored at lower energies, compared to the case of the ^{8}B projectile. However, because it actually becomes favored at energies which are still substantially above the barrier, where dynamic effects are supposedly not important, a static effect seems to be playing a role in the fusion enhancement for this system too. Further measurements and theoretical studies are needed in order to shed more light on this point.

A few words are in order about the possibility of having incomplete fusion (ICF) [27], a process where the ^{3}He projectile first breaks into ^{2}H + p and then either the deuteron or the proton fuses with ^{58}Ni. In that case, some of the measured protons could come from these processes and the $\sigma_{\rm fus}$ values in Table I would be misleading. From the projectile kinetic energy and the binding energy of the clusters, the available energy for fusion of each cluster can be estimated [28]. Considering the ^{2}H cluster for the present experiment, these energies turn out to be below the fusion barrier of the ^{2}H+^{58}Ni system, except at the highest measured energy, where the available energy is roughly on top of the barrier. It is thus highly improbable that this particular ICF process could compete with complete fusion (CF), where the whole projectile fuses with the target. In the latter process, the available energy for fusion is from 1 to 3 MeV above the corresponding barrier, depending on the bombarding energy. In addition, the low proton multiplicity ($\sim$0.8) associated with the ^{2}H+^{58}Ni fusion reaction tends to minimize the respective contribution to the proton spectra. The contribution from ICF to the spectrum of Fig. 1 for a ratio ICF/(CF + ICF) = 0.1, for instance, would be only 5%. As for ICF with the proton, this process is even less favorable than the previous one. The respective available energy for fusion in all cases is less than half the corresponding fusion barrier, which makes it negligible. Summarizing, ICF is highly improbable under the conditions of the present experiment, and the effect of any possible ICF event tends to be minimized in the proton spectra. Thus, it should be safe to associate the $\sigma_{\rm fus}$ values in Table I with CF.

IV. ELASTIC SCATTERING AND TOTAL-REACTION CROSS SECTIONS

Figure 5 shows the elastic scattering cross sections obtained at 12.7 MeV in the present work, along with the results of an optical model calculation. The dashed line corresponds to the global optical model potential in Ref. [29], but slightly modified to better fit the present data. This potential was derived from a large set of data for elastic scattering and reaction cross sections of ^{3}He on many target nuclei, covering a wide energy range. It uses the standard Woods-Saxon form factor for both the real and the imaginary parts, including volume and surface absorption, with a spin-orbit term of the Thomas form:

$$V(r,E) = V_C(r) + V_R(r,E) + i[W_S(r,E) + W_V(r,E)] + V_{\rm SO}(r)(\sigma \cdot l). \quad (1)$$

The diffuseness of the real volume term, a_R, and that of the imaginary surface term, a_S, were varied here to optimize the fit to the data (these parameters were kept fixed for all energies in Ref. [29]). All other parameters were obtained according to the prescription in Ref. [29] and are listed in Table II, which also includes the corresponding total-reaction cross section σ_R. The uncertainties reported for σ_R were estimated from the corresponding spread obtained by repeating the calculations with four additional optical model potentials which also gave good fits to the data.

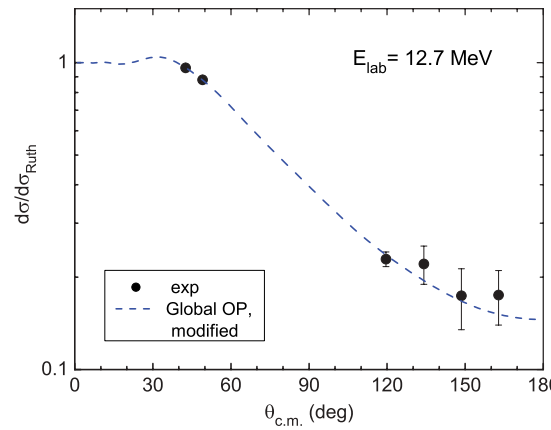

FIG. 5. (Color online) Elastic scattering angular distribution measured in the present work (symbols) and the results of an optical model calculation, described in the text (lines).

TABLE II. Energy-dependent parameters of the optical model potential [see Eq. (1)] and respective total-reaction cross sections. Fixed parameters calculated were $r_R = 1.15$ fm, $r_S = 1.21$ fm, $a_V = 0.66$ fm, $r_V = 1.62$ fm, $V_{SO} = 3$ MeV, $a_{SO} = 0.9$ fm, $r_{SO} = 1.27$ fm, and $r_C = 1.25$ fm. Radii are given by $R_x = r_x \times A_T^{1/3}$.

E_{lab} (MeV)	V_R (MeV)	a_R (fm)	W_S (MeV)	a_S (fm)	W_V (MeV)	χ^2/N	σ_R (mb)
12.0	135.9	0.70	30.8	0.78	0.0	0.85	616 ± 20
12.7	135.8	0.72	30.7	0.71	0.0	0.26	619 ± 22
19.5	134.3	0.78	29.5	0.78	0.011	0.41	1285 ± 43
21.9	133.8	0.76	29.1	0.82	0.254	1.35[a]	1431 ± 45
24.1	133.3	0.76	28.8	0.82	0.472	6.18[a]	1503 ± 47

[a]No absolute meaning for χ^2/N.

Additional elastic scattering data from the literature were analyzed with the method described above, with the purpose of studying the energy dependence of σ_R for the present system. Angular distributions at 12 MeV [30], 19.5 MeV [31], 21.9 MeV [32], and 24.1 MeV [34] are shown in Fig. 6. Because the uncertainties in the data points at 21.9 and 24.1 MeV are unknown, all points were given the same percentage weight in the fit by artificially assigning a 4% uncertainty to all points. The curves in Fig. 6 correspond to the potential parameters given in Table II, where the respective total-reaction cross sections are also indicated for each energy. Although feasible, a more complete coupled-channel analysis of these data is beyond the reach of the present work.

The calculated reaction cross sections are plotted in Fig. 7, along with the present fusion results. For $E_{c.m.} = 12.1$ MeV, where both σ_{fus} and σ_R were determined, it is clear that a substantial fraction of the total-reaction cross section ($\sim$30%) is not accounted for by fusion. It would be interesting to determine experimentally the contribution of transfer and/or breakup to this missing fraction. In particular, transfer processes with a positive Q value such as (^{3}He,α) ($Q = 8.36$ MeV) and (^{3}He,p) ($Q = 5.76$ MeV) should be investigated. One may speculate that the first process, involving a single-neutron pickup, might be quite important at low energies in the present system.

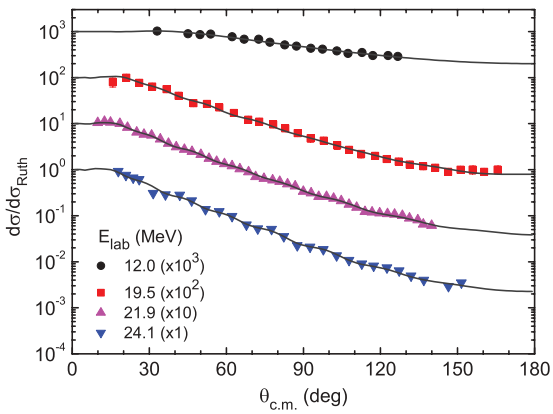

FIG. 6. (Color online) Elastic scattering angular distributions from the literature (symbols) and respective optical model calculations (lines) with the parameters given in Table II. Data are from [30] (12 MeV), [31] (19.5 MeV), [32] (21.9 MeV), and [34] (24.1 MeV).

The curves in Fig. 7 are drawn as a reference to establish possible similarities of $\sigma_R(E)$ with the behavior of either tightly bound nuclei (dotted line), weakly bound nuclei (solid line), or halo nuclei (dashed line). They correspond to Wong-type functions [35] deduced from the reduced curves that were obtained in Ref. [22] for each of these groups. Briefly, in this reference the experimental excitation functions for the total-reaction cross sections of a number of systems were plotted together in reduced form, using the scaling procedure mentioned above. This plot clearly showed that all systems were grouped along one of three trajectories, the highest lying one corresponding to systems with a halo projectile (^{6}He, ^{8}B), the intermediate one for weakly bound projectiles (^{6,7}Li, ^{7,9}Be), and the lowest one for the ^{16}O projectile. Enough targets and bombarding energies were analyzed to suggest this as a possible systematic behavior that may be valid also for other non analyzed systems.[1] Each trajectory could be characterized by a Wong function with reduced barrier parameters (see Ref. [10]), defined as $r_{0b} = R_0/r_{pt}$, $V_{Red} = V_0/(Z_p Z_t/r_{pt})$, and $\epsilon_0 = \hbar\omega_0/(Z_p Z_t/r_{pt})$. Here, R_0, V_0, and $\hbar\omega_0$ are the usual barrier parameters.

The corresponding parameter values of such reduced curves, compiled, for instance, in Ref. [7], are characterized by higher (lower) values of r_{0b} and ϵ_0 (V_{Red}) when going from tightly bound through weakly bound to halo systems. A possible physical interpretation of the above systematic behavior was suggested in Ref. [10] and further discussed in Ref. [23]. For instance, the shift of the halo-system cross sections to higher values, with respect to the quantities corresponding to tightly bound systems, is consistent with a static effect of the halo size, which "pushes" the barrier away to longer distances, at the same time lowering the barrier height. The longer tail of the nuclear density for weakly bound systems, with respect to tightly bound ones, could perhaps admit a similar interpretation for this case. The ϵ_0 parameter is related to the slope for falloff of the curves in the low-energy region. The larger values of ϵ_0 obtained for systems with

[1]Nine targets with a total of 32 points were analyzed for halo systems, three targets and 28 points for weakly bound systems, and one target and 13 points for the tightly bound projectile. However, in a later work where reactions of several projectiles with a ^{12}C target were considered, the separation between halo and weakly bound systems seems to disappear for this light target (see [36]).

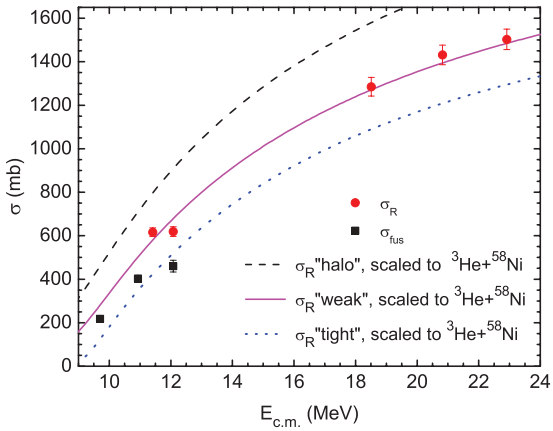

FIG. 7. (Color online) Total-reaction and fusion cross sections obtained in the present work (symbols). The meaning of the curves is explained in the text.

progressively weaker binding seems to be a signature for respective dynamic effects, which are known to occur in the sub-barrier region. In the context of the simple Wong model, such dynamic effects would be simulated by unrealistic narrow barriers.

The actual parameter values of the above-mentioned reduced curves (see, for instance, Ref. [7]), can thus be scaled to the ^{3}He+^{58}Ni system to produce the curves in Fig. 7. The respective values of R_0 (fm), V_0 (MeV), and $\hbar\omega_0$ (MeV) are 9.5, 8.2, and 4.5 for the dashed curve, 8.7, 8.6, and 3.6 for the solid curve, and 8.3, 9.2, and 1.5 for the dotted curve. As far as total-reaction cross sections are concerned, from this figure one can say that the ^{3}He projectile behaves like a weakly bound nucleus. This result was rather unexpected, as the original curve associated with weakly bound systems was obtained from data for projetiles of ^{6,7}Li and ^{7,9}Be [22]. These projectiles have binding energies much lower than that of ^{3}He. Further studies involving the latter projectile are necessary in order to further understand this point.

Implicit in the above observations is the fact that the reaction cross sections for ^{3}He+^{58}Ni are certainly enhanced with respect to more normal (tightly bound) nuclei, which would follow the dotted line in Fig. 7. The corresponding barrier, whose parameters were given above, should be associated with the total-reaction processes. When suitably reduced, the respective barrier height corresponds to $V_{\rm Red} = 0.82$. This is consistent with the value 0.83 estimated in Sec. III for the corresponding fusion barrier, which should be no lower than the total-reaction barrier. It could be even larger, though, but more data are needed in order to get a good experimental determination.

V. SUMMARY AND CONCLUSIONS

Proton-production cross sections were measured at backward angles for the ^{3}He+^{58}Ni system at three near-barrier energies. The respective proton spectra were shown to be consistent with the predictions of the evaporation model. Corresponding fusion cross sections were deduced and arguments were given that justify associating them with the CF process. The same type of arguments indicate that ICF is highly improbable at the measured bombarding energies.

A comparison with the fusion of other systems sharing the same target, in a plot of $\sigma_{\rm Red}$ vs $E_{\rm Red}$, indicates that the proton-halo projectile ^{8}B and the proton-rich nucleus ^{3}He share some common features. The data for both show an enhancement with respect to the fusion of the tightly bound nucleus ^{16}O. This enhancement seems to be caused by a static effect probably related to an extended nuclear size in both cases. While the enhancement continues up to the highest measured energies for ^{8}B, it gradually decreases with energy for the case of ^{3}He. The highest energy point for the latter projectile seems to fall on the path defined by the data for ^{16}O, i.e., there is no enhancement for this higher energy point.

An elastic scattering angular distribution also was measured at a single energy. An optical model analysis of this, along with additional data from the literature for four more energies, provided an excitation function for the total-reaction cross sections. Quite surprisingly, this excitation function follows the trend expected for very weakly bound systems, in spite of the moderately weak binding of ^{3}He. Further measurements and theoretical analyses are needed in order to shed more light on this.

ACKNOWLEDGMENTS

This work was partially supported by CONACYT (México) and by the NSF (USA) under Grant No. 09-69456.

[1] E. F. Aguilera, P. Amador-Valenzuela, E. Martinez-Quiroz, D. Lizcano, P. Rosales, H. García-Martínez, A. Gómez-Camacho, J. J. Kolata, A. Roberts, L. O. Lamm, G. Rogachev, V. Guimarães, F. D. Becchetti, A. Villano, M. Ojaruega, M. Febbraro, Y. Chen, H. Jiang, P. A. De Young, G. F. Peaslee, C. Guess, U. Khadka, J. Brown, J. D. Hinnefeld, L. Acosta, E. S. Rossi Jr, J. F. P. Huiza, and T. L. Belyaeva, Phys. Rev. Lett. **107**, 092701 (2011).
[2] L. C. Vaz, J. M. Alexander, and G. R. Satchler, Phys. Rep. **69**, 373 (1981).
[3] M. Beckerman, Rep. Prog. Phys. **51**, 1047 (1983).
[4] M. Dasgupta, D. Hinde, N. Rowley, and A. Stefanini, Annu. Rev. Nucl. Part. Sci. **48**, 401 (1998).
[5] N. Keeley, R. Raabe, N. Alamanos, and J. L. Sida, Prog. Part. Nucl. Phys. **59**, 579 (2007).
[6] E. F. Aguilera and J. J. Kolata, Phys. Rev. C **85**, 014603 (2012).
[7] E. F. Aguilera, J. Phys.: Conf. Ser. **387**, 012001 (2012).
[8] H. Esbensen and G. F. Bertsch, Phys. Rev. C **66**, 044609 (2002).
[9] E. F. Aguilera, J. J. Kolata, and L. Acosta, Phys. Rev. C **81**, 011604(R) (2010).
[10] E. F. Aguilera, I. Martel, A. M. Sánchez-Benítez, and L. Acosta, Phys. Rev. C **83**, 021601(R) (2011).
[11] A. Gavron, Phys. Rev. C **21**, 230 (1980).
[12] M. Y. Lee, F. D. Becchetti, T. W. O'Donnell, D. A. Roberts, J. A. Zimmerman, V. Guimarães, J. J. Kolata, D. Peterson, P. Santi,

P. A. DeYoung, G. F. Peaslee, and J. D. Hinnefeld, Nucl. Instr. Methods Phys. Res. A **422**, 536 (1999).
[13] R. G. Stokstad, in *Treatise on Heavy-Ion Science*, edited by D. A. Bromley (Plenum Press, New York, 1985), Vol. 3, p. 83.
[14] A. Gilbert and A. G. W. Cameron, Can. J. Phys. **43**, 1446 (1965).
[15] J. Gomez del Campo and R. G. Stokstad, ORNL Report TM-7295 (1981).
[16] J. Gomez del Campo (2001), private communication.
[17] A. Gavron, *Computational Nuclear Physics 2. Nuclear Reactions*, edited by K. Langanke, J. A. Maruhn, and S. E. Koonin, (Springer, New York, 1993), p. 108.
[18] N. Keeley, J. S. Lilley, J. X. Wei, M. Dasgupta, D. J. Hinde, J. R. Leigh, J. C. Mein, C. R. Morton, H. Timmers, and N. Rowley, Nucl. Phys. A **628**, (1998).
[19] P. R. S. Gomes, J. Lubian, I. Padron, and R. M. Anjos, Phys. Rev. C **71**, 017601 (2005).
[20] L. F. Canto, P. R. S. Gomes, J. Lubian, L. C. Chamon, and E. Crema, J. Phys. G: Nucl. Part. Phys. **36**, 015109 (2009).
[21] L. F. Canto, P. R. S. Gomes, J. Lubian, L. C. Chamon, and E. Crema, Nucl. Phys. A **821**, 51 (2009).
[22] J. J. Kolata and E. F. Aguilera, Phys. Rev. C **79**, 027603 (2009).
[23] E. F. Aguilera, J. J. Kolata, I. Martel, A. M. Sánchez-Benítez, and L. Acosta, *Proceedings of the XXXIV Edition of the Brazilian Workshop on Nuclear Physics*, Foz de Iguaçu, Parana State, Brazil (2011); PoS(XXXIV BWNP)009.
[24] R. K. Puri and R. K. Gupta, in *Heavy Ion Fusion: Exploring the Variety of Nuclear Properties; Proceedings, International Conference, Padova, 1994*, edited by A. M. Stefanini, G. Nebbia, S. Lunardi, G. Montagnoli, and A. Vitturi (World Scientific, Singapore, 1994), p. 319.
[25] I. Dutt and R. K. Puri, Phys. Rev. C **81**, 064608 (2010).
[26] I. Tanihata, H. Hamagaki, O. Hashimoto, S. Nagamiya, Y. Shida, N. Yoshikawa, O. Yamakawa, K. Sugimoto, T. Kobayashi, D. E. Greiner, N. Takahashi, and Y. Nojiri, Phys. Lett. B **160**, 380 (1985).
[27] A. Diaz-Torres, J. Phys. G: Nucl. Part. Phys. **37**, 075109 (2010).
[28] E. F. Aguilera, E. Martinez-Quiroz, P. Rosales, J. J. Kolata, P. A. DeYoung, G. F. Peaslee, P. Mears, C. Guess, F. D. Becchetti, J. H. Lupton, and Yu Chen, Phys. Rev. C **80**, 044605 (2009).
[29] Y.-L. Xu, H.-R. Guo, Y.-L. Han, and Q.-B. Shen, Sci. China Phys. Mech. Astron. **54**, 2005 (2011).
[30] J. L. Yntema, B. Zeidman, and R. H. Bassel, Phys. Lett. **11**, 302 (1964).
[31] R. Bock, P. David, H. H. Duhm, H. Hefele, U. Lynen, and R. Stock, Nucl. Phys. A **92**, 539 (1967).
[32] D. D. Armstrong, A. C. Blair, and R. H. Bassel, cited as private communication in Ref. [33].
[33] E. F. Gibson, B. W. Ridley, J. J. Kraushaar, and M. E. Rickey, Phys. Rev. **155**, 1194 (1967).
[34] T. Fujisawa, H. Kamitsubo, T. Wada, and M. Igarashi, J. Phys. Soc. Jpn. **27**, 278 (1969).
[35] C. Y. Wong, Phys. Rev. Lett. **31**, 766 (1973).
[36] A. Barioni, J. C. Zamora, V. Guimarães, B. Paes, J. Lubian, E. F. Aguilera, J. J. Kolata, A. L. Roberts, F. D. Becchetti, A. Villano, M. Ojaruega, and H. Jiang, Phys. Rev. C **84**, 014603 (2011).